Journal of Magnetism and Magnetic Materials 593 (2024) 171881

Contents lists available at ScienceDirect

Journal of Magnetism and Magnetic Materials

journal homepage: www.elsevier.com/locate/jmmm

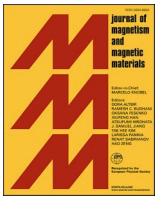

Influence of nanoparticles morphology in magnetic fluids

A. Gómez [a], A. Barón [b], J. Berasategi [a], M. Blanco [c], A. García [d], J. Gutiérrez [d,e,*], D. Iglesias-Rojas [b], M. Insausti [b], S. Lanceros-Mendez [d,f], C.R. Tubio [d], M.M. Bou-Ali [a]

[a] Fluid Mechanics Group, Mondragon University, 20500 Arrasate-Mondragón, Spain
[b] Dept. Organic and Inorganic Chemistry, Faculty of Science and Technology, University of the Basque Country UPV/EHU, Barrio Sarriena s/n, 48940 Leioa, Spain
[c] Surface Chemistry & Nanotechnologies Unit, Fundación Tekniker, Iñaki Goenaga 5, 20600 Eibar, Spain
[d] BCMaterials, Basque Center for Materials, Applications and Nanostructures, UPV/EHU Science Park, 48940 Leioa, Spain
[e] Dept. Electricity and Electronics, Faculty of Science and Technology, University of the Basque Country UPV/EHU, Barrio Sarriena s/n, 48940 Leioa, Spain
[f] IKERBASQUE, Basque Foundation for Science, 48009 Bilbao, Spain

ARTICLE INFO

Keywords:
Magnetite
Magnetic nanoparticles
Morphology
Magnetorheological fluids

ABSTRACT

In this work magnetic fluids at two different volume concentrations (5 % and 10 %) of magnetite nanoparticles of different morphologies and sizes (octahedral, 38 ± 5 nm; truncated octahedral, 10 ± 1 nm; rod-like, 95 nm x 10 nm; spherical 33 ± 20 and 90 ± 10 nm) have been formulated (by using mineral oil as liquid carrier and Aerosil®300 as viscosity-controller agent) and fabricated. The obtained results allow us to conclude that: a) the fluid with 10 %vol concentration spherical nanoparticles presents the highest magnetorheological response observed in this study, over a 4000 % change of yield stress with the maximum applied field strength. This is due both to their highest magnetic saturation and an effective nanoparticle clustering; b) the fluid based on octahedral particles shows a good balance between magnetorheological response (up to a 795 % change of yield stress) and reversibility (up to a 92 %), which indicates the competitiveness of these particles for the formulation of magnetic fluids. On the contrary, truncated octahedral nanoparticles, although maintaining that high reversibility capability, present a poor MR response (75–95 % change of yield stress for 5 and 10 %vol. concentrations); c) the poor magnetorheological response observed and non-expected reversibility behavior obtained for rod-like particles indicate that further deepening of the understanding of their dispersion and internal structuring is needed.

1. Introduction

Magnetic fluids consist mainly of magnetic particles suspended in a carrier liquid. These type of fillers own an inherent magnetic moment, but in the absence of a magnetic field the interaction between particles is practically non-existent and therefore the behavior of this magnetic fluid can be approximated to the Newtonian behavior, if the magnetic filler concentration is low enough. Nevertheless, when a magnetic field is applied to such fluid the magnetic moments within the particles will rotate in order to align parallel along the field. Now one individual particle with its net magnetic moment will generate a magnetic dipolar interaction with neighboring magnetic particles, and the magnetic particles within the magnetic fluid will align themselves creating so chain-like structures. As a result, the rheological behavior of a magnetic fluid can be modified in a controlled and reversible way by an external magnetic field, being now referred as a magnetorheological (MR) or intelligent/smart magnetic fluid [1–3]. The observed magnetic field dependent rheology manifest itself as substantial changes in the viscosity of the magnetic fluid accompanied by high values of the yield-stress (or stress needed to break the chain-like structures of the magnetic particles) and a pseudo-plastic post-yield behavior [4].

One of the first classifications of magnetic fluids was carried out by considering the particle size: ferrofluids (FF) composed of nanoparticles, and magnetorheological fluids (MR) based on microparticles [5]. Traditionally, micrometer sized magnetic particles had a considerably higher magnetic saturation than magnetic nanoparticles. Because the magnetic field-induced stresses are expected to grow quadratically with the magnetic saturation of the particles, MR fluids presented a higher magnetorheological response than FF and most industrial applications (as variable dampers or brakes [6]) were mainly based on MR fluids rather than FF.

Stability of the fabricated MR fluid is also an important task [2]. After the removal of the magnetic field, the fluid will return to a situation that will depend on the remnant magnetization of the magnetic

* Corresponding author at: BCMaterials, Basque Center for Materials, Applications and Nanostructures, UPV/EHU Science Park, 48940 Leioa, Spain.
E-mail address: jon.gutierrez@ehu.eus (J. Gutiérrez).

https://doi.org/10.1016/j.jmmm.2024.171881
Received 26 October 2023; Received in revised form 16 February 2024; Accepted 16 February 2024
Available online 17 February 2024

filler. Only when those are superparamagnetic and the magnetic field is removed, the fluid will truly return to its initial configuration. To achieve this, it is necessary to avoid sedimentation of the solid phase and irreversible aggregates between magnetic particles, caused by the direct contact among them in the presence of the magnetic field. For this last there are widely known strategies to avoid such stability problems as the use of surfactants, gelling additives and/or polymeric coatings. Considering the micrometer particle size of the very first fabricated MR fluids, Brownian motion was not sufficient to avoid the sedimentation of the solid filler particle phase. The long-term stability of MR fluids has been recently improved with the progress made in the synthesis of magnetic nanoparticles with high magnetic saturation [7,8]. Nanoparticles within a fluid tend to settle more slowly and even remain indefinitely suspended by Brownian motion. Thus, a new field has been opened in the development of stable magnetic fluids based on nanomagnetic fillers with enhanced MR response.

As presented, MR fluids response depends mainly in the size, magnetization and volume fraction (commercial MR fluids contain usually a 30–40 %vol. of particle within the suspension) of the magnetic filler. Few studies have reported about the magnetic particle shape influence in MR fluids [9,10], but obtained results indicate that when using elongated magnetic particles instead of the classical spherical ones lead to better MR behavior (higher yield stress) and reduction of sedimentation degree [11–13]. The dimensions of the particles used in these studies ranged from 0.7 μm diameter for the spherical shaped to 7 μm x 0.7 μm for the rod-like ones.

To advance the understanding and development of stable, highly responsive magnetic fluids, it is necessary to focus in how the morphology of the magnetic nanofillers may affect the behavior of these MR fluids. Bearing this in mind, in this work we present results obtained for magnetic fluids fabricated with in-house synthesized magnetite nanoparticles with three different shapes: octahedral, truncated-octahedral and rod-like. Additionally, commercially available spherical magnetite nanoparticles have been also employed. The morphology and the magnetic properties of the four types of magnetite nanoparticles is shown further down. Magnetic fluid samples with two different concentrations (5 % and 10 % by volume) will be fabricated. The rheological behavior of these fluids will be analyzed by measuring flow curves at different applied magnetic field intensities. To analyze the rheological behavior observed, the yield stress, consistency and the pseudo-plasticity index parameters were evaluated for each particle shape and concentration within the MR fluid. In addition, the mechanisms of rupture of the magnetic field induced inner structures of the nanoparticles have been analyzed by considering the dimensionless viscosity as a function of the dimensionless Mason number. Finally, the degree of reversibility of the hereby studied MR fluids will be analyzed by measuring flow curves in the absence of magnetic field, before and after the application of a magnetic field with different intensities.

2. Materials and methods

2.1. Synthesis and first characterization of the nanoparticles

Four types of particles have been used in this study: octahedral (Oct), truncated octahedral (Oct-T), rod-like (NRd) and spherical (Sphe). The first three have been specifically synthesized in-house, while the spherical particles were purchased from the commercial supplier Sigma-Aldrich.

Octahedral particles were synthesized by thermal decomposition from the previously obtained iron (III) oleate precursor [14,15]. 9.027 g. of Fe(oleate)3 were added to a mixture of 10 ml benzyl ether, 20 ml octadecene and 6.4 ml oleic acid that was maintained in a three neck round bottom flask. The reaction was carried out under continuous N_2 flux and mechanical stirring while the temperature of the reactor was increased first until 190 °C at 10 °C/min and secondly up to 320 °C at 3°/min., where it was maintained under contimuous reflow for 60 min. A black power precipitated and was cleaned by centrifugation (22000 rpm at 6 °C) adding THF and ethanol in a 10:20 ml relation. The final product was redispersed in chloroform.

These nanoparticles present an octahedral morphology with an average size of 38 ± 5 nm. Nevertheless, some polydispersity can be observed in the micrograph, as there some diversity in the particle' sizes. X-ray diffraction (XRD) pattern shows the absence of secondary phaseses, as it shows an excellent match with the pattern of inverse spinel structure of Fe_3O_4. Additionally, the crystallite size obtained from the maximum peak in XRD (311), 37 ± 2 nm, is in good accord with the morphological size, and so we concluded that the particles are single crystals. The magnetic saturation shown by the magnetic core of the particles is 85 Am^2/kg and has been calculated after correcting the organic amount coating the nanoparticles (which is 8.3 % and was obtained from thermogravimetry measurements). Magnetic saturation is very close to the value observed for bulk magnetite (92 Am^2/kg at room temperature).

Truncated octahedral particles were synthesized by coprecipitation [16]: 24 mmol of $FeCl_3$ and 12 mmol of $FeSO_4{\cdot}7H_2O$ have been dissolved in 300 ml of water and kept under nitrogen (N_2) atmosphere and in constant agitation at 90 °C for one hour to achieve good homogenization. Then, a 100 ml solution of 2.5 M NaOH was added drop by drop, maintaining constant agitation to achieve the precipitation of the particles. Finally, the solution is filtered and the magnetite extracted was washed several times with deionized water and dried in a furnace at 100 °C overnight. The truncated octahedral particles presented an irregular shape and an average size of 10 ± 1 nm. XRD results showed that there were no secondary phases but only pure magnetite, and it is concluded that the particles are single crystals. The magnetic saturation shown by these particles is 60 Am^2/kg.

Rod-shaped particles were synthesized using the solvothermal method. The synthesis was adapted from Si *et al.* [17]. First, 2.65 g of hexadecylamine and 26.65 ml of oleic acid were dissolved in 106.65 ml of 1-octanol at 50 °C under magnetic stirring. After homogenization of the solution, it was cooled down to room temperature. Subsequently, 26.65 ml of $Fe(CO)_5$ were added, and the solution was further stirred for another 5 min. Finally, it was poured into a 250 ml Teflon autoclave, sealed and heated at 200 °C for 6 h inside a preheated oven, where it was kept for 6 h. The autoclave was left to cool down after the 6 h. The resulting product was washed with ethanol three times and re-dispersed in chloroform. Rod-type particles have a cylindrical morphology in which the longitudinal dimension (95 nm) is considerably larger than the transverse dimension (10 nm). The magnetic hysteresis loop of the sample was measured, obtaining a saturation magnetization of M_S = 40.7 Am^2/kg.

The spherical nanoparticles used in this study were commercially sourced from Sigma-Aldrich (ref 637106—97 % Fe_3O_4). From the information given by Sigma-Aldrich, they delivered cubic magnetite with an Fd3m (227) space group, in agreement with the JCPDS card number 19–629. From TEM images, we have found a mixture of small and big particles with particle size ranges 33 ± 20 nm and 90 ± 10 nm, but with not strictly spherical shape (see Fig. 4, left). The supplied power exhibits a magnetic saturation of 95 Am^2/kg.

Table 1 summarizes the average size (estimated from TEM observations) as well as the main magnetic parameters obtained for the different nanoparticles employed in this work.

From this magnetic characterization, we can elucidate the single- or multi-domain character of our magnetite nanoparticles after a careful analysis of the measured magnetic saturation M_S, coercive field H_C and remnant magnetization M_R [18] values. The small particle size together with the high magnetic saturation and low remanence and coercive fields (null or almost null) hint for single domain nanoparticles for octahedral and truncated octahedral shaped nanoparticles. These last also show superparamagnetic behavior with absence of remanence and coercive field. For the nanorod shaped magnetite nanoparticles, the combination of their size (90 nm length) with low magnetic saturation

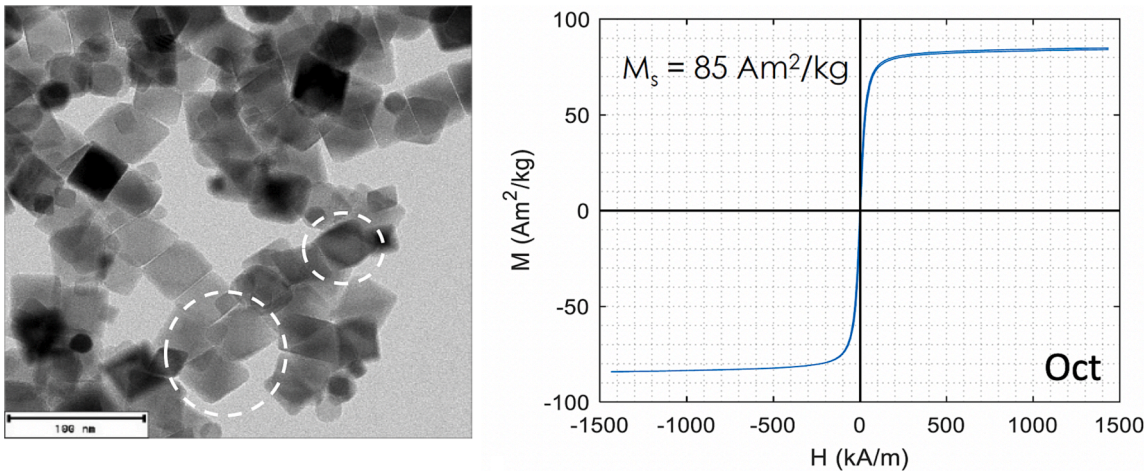

Fig. 1. Octahedral magnetite particles: *(left)* TEM image (dashed circles indicate clearly seen octahedral particles); *(right)* magnetization hysteresis loop. Measurements performed at room temperature.

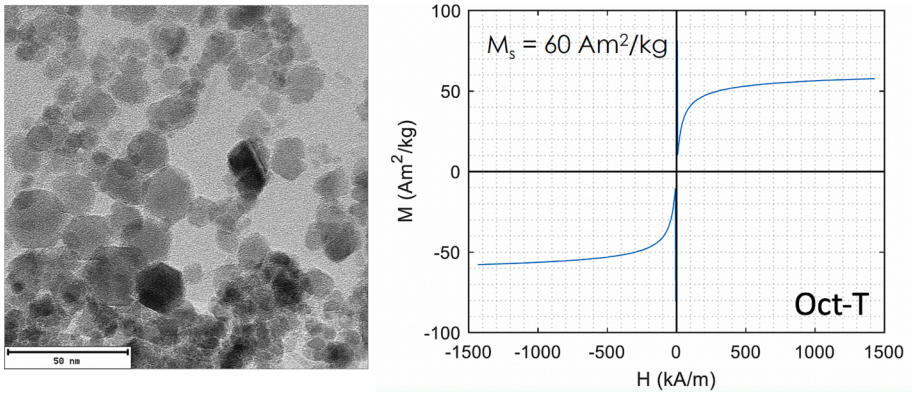

Fig. 2. Truncated octahedral magnetite particles: *(left)* TEM image; *(right)* magnetization hysteresis loop. Measurements performed at room temperature.

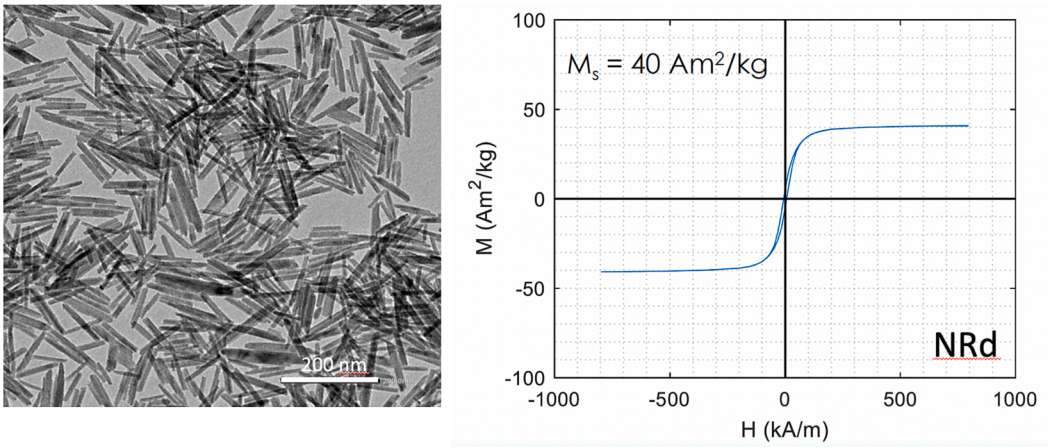

Fig. 3. Rod-like magnetite particles: *(left)* TEM image; *(right)* magnetization hysteresis loop. Measurements performed at room temperature.

and remanence together with its moderate coercive field make more probably for then to be also single domain nanoparticles. Finally, the case of spherical magnetite nanoparticles is just the opposite, with the mixture of small and big particle sizes, but clearly high magnetic saturation and also high remanence and coercive field. That is, commercially purchased magnetite powders are magnetic multidomain nanoparticles.

2.2. Fabrication and characterization of the magneto-rheological fluids

The fabrication of the magnetic fluids analyzed started with the corresponding amount of the liquid carrier, in this case mineral oil. Next, the viscosity-controller agent Aerosil®300 was added in the ratio of 1 g Aerosil®300 per 40 g mineral oil. The mixture was then homogenized in two steps. First, by ultrasonic agitation for 5 min with a Transonic TI-H. Afterwards, by mechanical agitation for 5 min with a Heidolph RZR

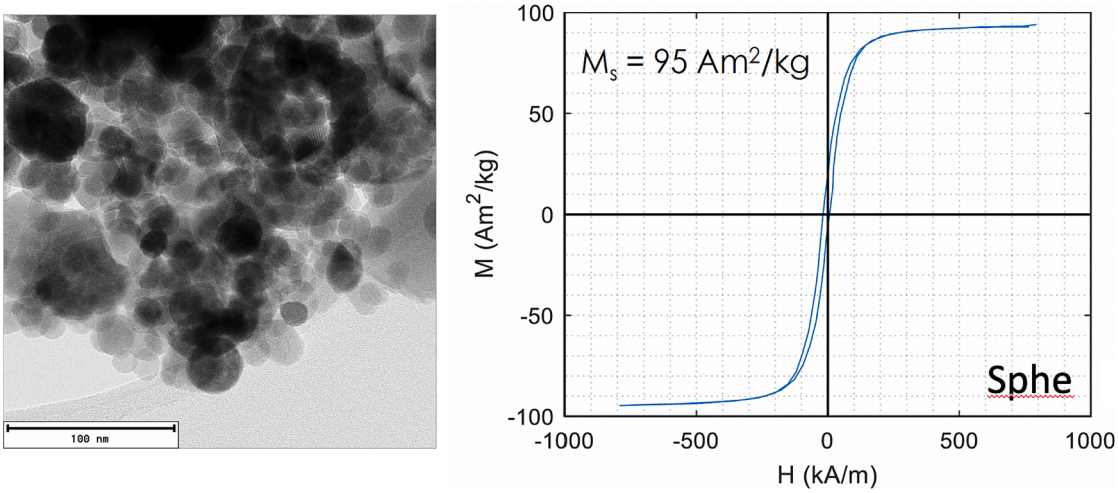

Fig. 4. Spherical magnetite particles: *(left)* TEM image; *(right)* magnetization hysteresis loop. Measurements performed at room temperature.

Table 1
Size and magnetic properties comparison of the different origin magnetite nanoparticles used in this work.

Nanoparticle morphology	Size (nm)	M_S (Am^2/kg)	M_R (Am^2/kg)	M_R / M_S	H_C (kA m^{-1})
Octahedral (Oct)	38 ± 5	85	9	0.106	2.5
Truncated octahedral (Oct-T)	10 ± 1	60	≈ 0 (*)	0	≈ 0 (*)
Rod-shaped (NRd)	Length: 95 Diameter: 10	40.7	5.7	0.14	6.6
Spherical (Sphe)	33 ± 20 90 ± 10	95	21.5	0.226	20

(*) superparamagnetic nanoparticles.

2051. In the next step, the surfactant was added in the desired concentration for the amount of nanoparticles to be added. In this case, 28.49 mg of oleic acid was used per 1 g of nanoparticles. Finally, the nanoparticles were added in two steps: first, 50 % of different nanoparticles were added to the previously prepared carrier mixture and dispersed by 5 min of ultrasound stirring, followed by 5 min of mechanical stirring. Then, the remaining particles were added next and 12 h of ultrasound stirring followed by a subsequent 12 h of mechanical stirring were applied for a better dispersion. Two different concentrations of 5 and 10 % vol. of magnetite nanoparticles content were used for all the different shapes, and the correspondent fluids fabricated.

The rheological characterization of the magnetic fluids was performed using an MCR-501 rotational rheometer with a 20 mm parallel plate configuration. An MRD 70/1T cell was used for the application of the magnetic field. The test is composed of three intervals. In the first one, the plate rotates at a constant speed of 140 rpm during 30 s for sample homogenization. In the second interval, the corresponding magnetic field is applied, and the sample is waited for 30 s are allowed for the sample to stabilize its internal structuration. The third interval is the characterization itself, where a shear rate sweep is performed from 0.01 to 600 s^{-1} in 60 logarithmically spaced intervals, each interval with a duration of three seconds. Shear rate sweeps were measured at seven different magnetic fields, starting with a zero magnetic field, and increasing up to a maximum strength of 616 kA/m. All these rheological characterization measurements were performed at 25 °C, being the temperature controlled by means of a Refrigerated Heating Circulator Julabo F 25-MC.

During the test, rotational speed and torque data are collected. As the stress state of the sample is not uniform and the behavior of magnetic fluids is expected to be non-Newtonian, the conversion from physical to rheological parameters is performed by using Rabinowitsch conversion.

The obtained experimental results were fitted to the Herschel-Bulkley fluid model [19], a general model that is commonly used for magnetic fluids because it is defined by a yield-stress and a pseudo-plastic post-yield behavior. The model is described by equation (1), where τ is the shear stress, τ_0 is the yield stress, k is the consistency factor, $\dot{\gamma}$ is the shear rate and n is the pseudo-plasticity index:

$$\tau = \tau_0 + k \bullet \dot{\gamma}^n \quad (1)$$

To analyze the reversibility of all the magnetic fluids studied, once the flow curve for each corresponding magnetic strength is obtained, the fluid followed a demagnetizing process and the rheological behavior at zero applied field was measured once again. By following this procedure, the capability of each fluid to recover its initial rheology behavior can be easily evaluated.

Finally, the magnetic filler size distribution as well as their packing fraction (aggregates presence) was measured directly in the fabricated MRF fluids by performing Small Angle X-rays (SAXS) measurements. These were obtained by using a Rigaku Smartlab automatic diffractometer operating at 40 kV and 50 mA. The 2θ scans in transmission mode were obtained with parallel bean configuration (CBO), standard holder, vacuum path, automatic attenuator and 1-D DteX250 detector. The measured data were collected in continues mode, from 0.06 to 8° step size of 0.02° at 0.13°/min scan speed.

3. Results and discussion

3.1. Magnetorheological behavior of the fabricated fluids

Flow curves for all the synthesized fluids were measured when applying seven different values of the magnetic field strengths. All of them showed a strong magnetorheological response, with increasing shear stress values as the magnetic field strength increased. This trend maintains until the magnetic saturation of the magnetic fillers, above which the fluid exhibits minimal variations. Additionally and at high magnetic fields, a series of irreversible aggregates can be formed. They will have impact in the rheological behavior of the fluids, and further details on this observation will be discussed later.

The measurement error varies with the applied shear rate, decreasing from a maximum of 6.4 % at 0.01 s^{-1} to 0.55 % at 600 s^{-1}. The sample was measured five times, and the error range remains consistent regardless of the applied magnetic field. As an example, the experimental rheological behavior of the magnetic fluid containing 10 %vol.

content of spherical magnetite nanoparticles can be seen in Fig. 5 (curves for the other fabricated fluids behave similarly). The fit of experimental results to the Herschel-Bulkley model (equation (1) is excellent, with a minimum correlation coefficient $R^2 = 0.99$ for all fluids analyzed and magnetic fields analyzed.

The results of all the flow curves measured for all fabricated MR fluids were analyzed by determining the three parameters of the Herschel-Bulkley post-yield model. Each parameter will be analyzed, in the following, considering nanoparticle morphology, content and magnetic behavior.

First, let us consider the yield stress τ_0. This is doubtless one of the most important properties when dealing with applications of MR fluids [20]. All our analyzed MRFs showed the same trend with values increasing faster than linear with respect to concentration (see Fig. 6). Thus, the yield stress value reaches almost its maximum value when 140.1 kA/m magnetic field is applied, and remains practically constant for fields higher than 280.9 kA/m. This observation fully correlates with the previously measured magnetic hysteresis loops (see Figs. 1 to 4), in which the magnetic saturation of each nanoparticle is reached for a magnetic field intensity of 280.9 kA/m. As a first consequence, the magnetic nanoparticles within each fluid interact among themselves with the maximum possible magnetic dipolar interaction, forming the strongest inner columnar structures. Table 2 summarizes these measured yield stress values.

Differences in the yield stress of the studied fluids are also affected by the size, geometry and number of the filler magnetic particles. Fig. 7 shows the measured yield stress values at zero applied magnetic field as a function of the saturation magnetization of each magnetic filler. Results obtained for all the studied MR fluids are shown. As observed, the yield stress trend is similar for both 5 %vol. and 10 %vol. magnetic filler concentrations.

As presented in data of Table 2 and Fig. 7, in all particles that exhibit a certain degree of sphericity (spherical, octahedral, and truncated octahedral), the yield stress (τ_0 (Pa) at 0 kA/m) of the fluid increases as the particle size decreases. A qualitatively explanation can be given if we assume the spherical and octahedral geometries to show the same demagnetizing factor of just a spherical nanoparticle (≈ 0.333) [21], so the effect of any applied magnetic field will be similar for both of them. Besides, saturation magnetization values are quite similar (see Table 1). All this, together with a similar concentration of magnetic fillers (in the range 1–2 x 10^{15} particles/mL) led to our observations of the lowest measured yield stress values for these nanoparticles geometries. From our measurements, MR fluids containing spherical particles showed the lowest yield stress (only 4.9 Pa) without magnetic field.

The situation for the fluid containing truncated octahedral nanoparticles is similar: in this case saturation magnetization is moderate (60 Am^2/kg) but being the smallest nanoparticle studied, the concentration of magnetic fillers (in the range 0.5–1 x 10^{17} particles/mL) is the highest among all analyzed MR fluids. As a first consequence, this will cause still a greater interaction between NPs and therefore the observed highest yield stress among the different nanoparticle morphologies.

We previously described at the Introduction section that the use of elongated magnetic fillers instead of spherically shaped ones usually leads to a higher yield stress value (see, for example, references [12,13]). This has not been our case, since being the concentration of magnetic nanorods within the MR fluid similar (1.6–3.3 x 10^{15} particles/mL), their saturation magnetization is low (just 40.7 Am^2/kg). The combination of both facts makes our measured yield stress values to be slightly lower than for the MR fluids containing octahedral nanoparticles.

In which concerns the consistency factor k, this is directly related to the viscosity of the fluid and depends on the flow curve curvature exponent n [22]. For this, to make a proper comparison among the different MR fluids studied in this work, it is necessary to simultaneously account for the consistency parameter k (Fig. 8) and the pseudo-plasticity index n (Fig. 9). In our study, pseudoplasticity indexes fall within the range of $0.5 < n < 1$ for all the flow diagrams obtained, which ensures the pseudo-plastic behavior accompanied by shear-thinning of our fluids. Besides, n seems to be practically independent of the particle concentration.

MR fluids containing octahedral and spherical nanoparticles are the best and clearest in their behavior respect to the application of the magnetic field: we observed a minimum value of the consistency in the absence of magnetic field and a significant increase at low magnetic fields, that is followed by a saturation value above 280.9 kA/m and up to 616.7 kA/m. At the same previous applied magnetic fields, the n parameter behaves in the same manner for both fluids: high initial value (at 0 kA/m) that quickly decreases to half the value (from 280.9 kA/m

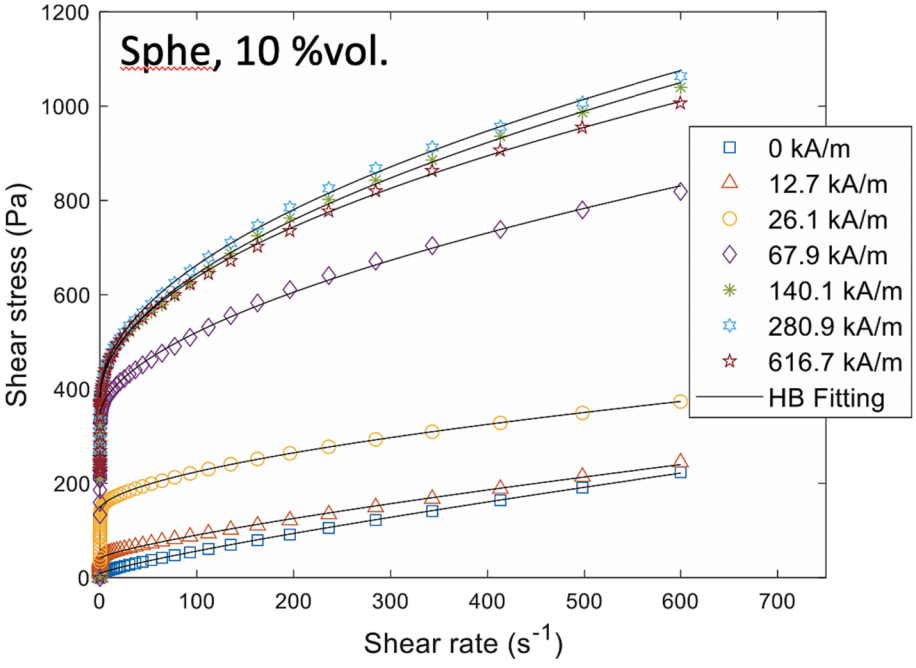

Fig. 5. Flow curves of the magnetic fluid containing 10 % vol. spherical magnetite particle concentration. Measurements performed at room temperature.

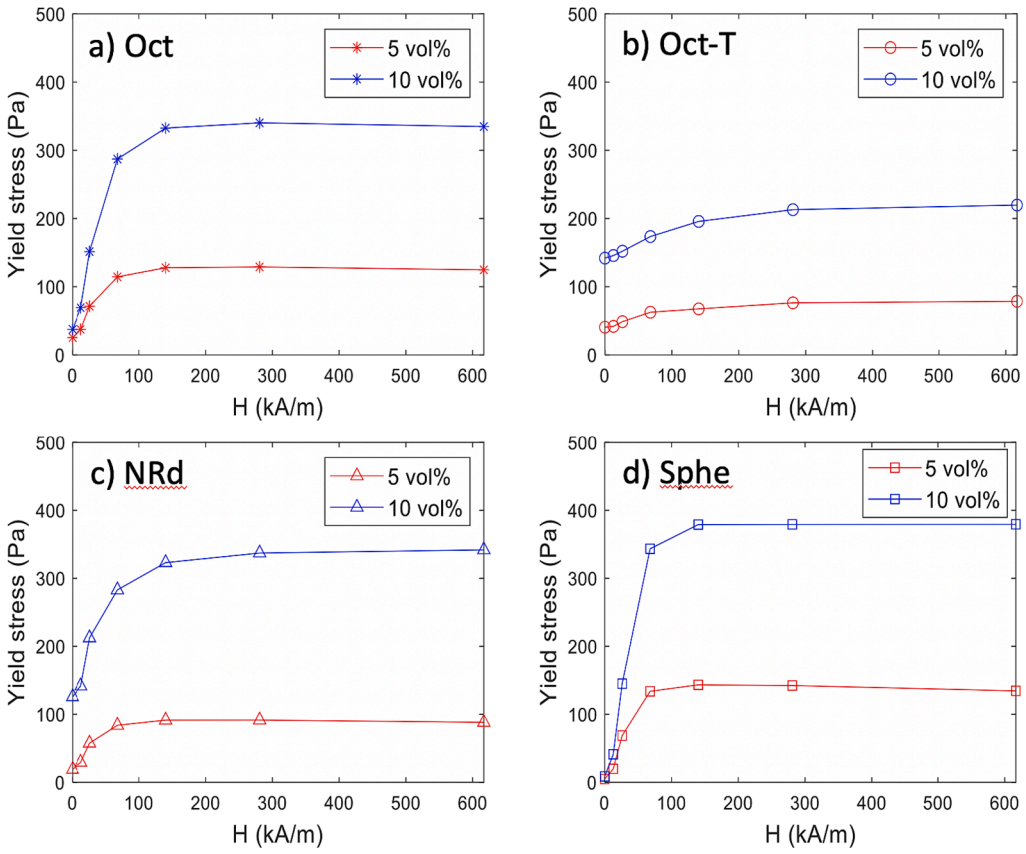

Fig. 6. Yield stress values plotted against the applied magnetic field for two different concentrations of all nanoparticles studied: a) octahedral; b) truncated octahedral; c) rod-shaped; d) spherical. Measurements performed at room temperature.

Table 2
Yield stress values for the studied different magnetic fluids and concentrations, measured at minimum (zero) and maximum (616.7 kA/m) applied magnetic fields.

Particles shape	% vol.	τ_0(Pa) at 0 kA/m	τ_0(Pa) at 616.7 kA/m	$\Delta\tau_0$(%)
Octahedral	5	25.3	124.7	392.9
	10	37.4	334.8	795.2
Truncated octahedral	5	40.6	78.6	95
	10	141.9	219.7	77.8
Rod-shaped	5	19.1	88.2	361.8
	10	125.9	341.8	171.5
Spherical	5	4.9	134.5	2644.5
	10	8.7	379.4	4260.9

and beyond). This behavior is roughly followed by the MR fluid containing nanorods as magnetic particle fillers: there is an initial dispersion (at low applied magnetic field strengths) of both consistency and pseudo-plasticity index, followed by saturated values above 140.1 kA/m. Showing zero applied magnetic field yield stress values of 19.1 and 125.9 Pa (almost 10 times higher) for 5 %vol. and 10 %vol. concentrations respectively, should prevent the spontaneous formation of columnar-like structures within these fluids, despite this type of nanoparticles having the lowest saturation magnetization of (40.7 Am^2/kg) for all the particles used in this study.

Finally, the previous described similarity in behavior is not evident for the fluid containing truncated octahedral magnetite nanoparticles. Furthermore, for this fluid the consistency values show a clear linear dependence, not significantly with the applied magnetic field strength and are independent of concentration. At the same time, the pseudo-plasticity index smoothly decreases continuously (see Fig. 8b and 9b).

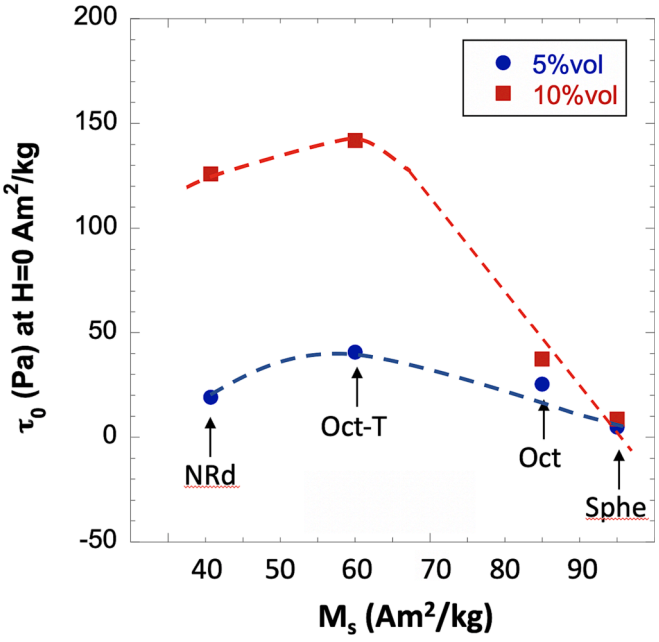

Fig. 7. Yield stress values measured at zero applied magnetic field plotted as a function of the saturation magnetization of each magnetic filler. Measured values for both 5 %vol. and 10 %vol. magnetic filler concentrations are shown. Measurements performed at room temperature.

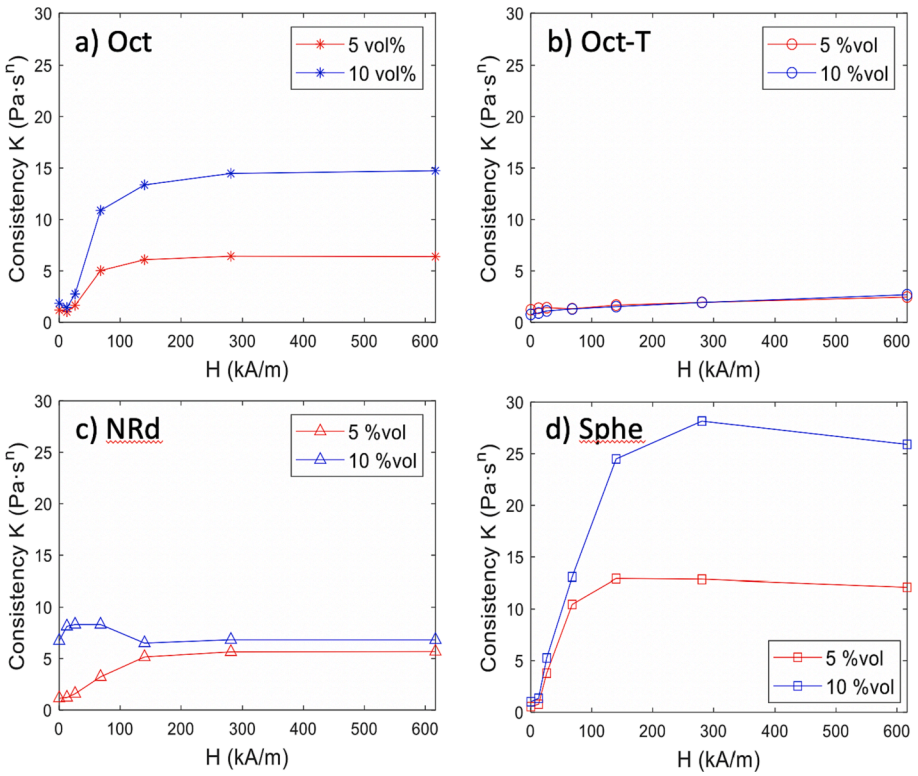

Fig. 8. Consistency index *k* values plotted against the applied magnetic field for two different concentrations of all nanoparticles studied: a) octahedral; b) truncated octahedral; c) rod-shaped; d) spherical. Measurements performed at room temperature.

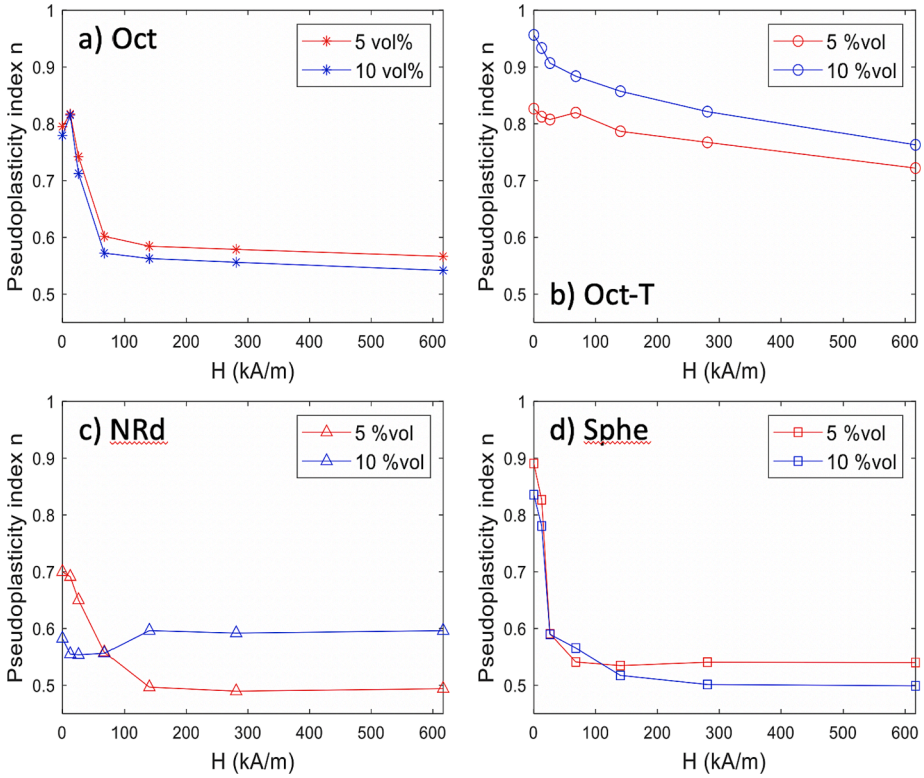

Fig. 9. Pseudoplasticity index *n* values plotted against the applied magnetic field for two different concentrations of all nanoparticles studied: a) octahedral; b) truncated octahedral; c) rod-shaped; d) spherical. Measurements performed at room temperature.

The small change observed in the yield stress (for zero and maximum applied magnetic field strengths) of only 95 % and 77.8 % for 5 %vol. and 10 %vol. concentrations respectively could be an indication of the formation of permanent nanoparticles agglomerates, that do not disappear when the applied magnetic field is removed. Like it happened with the MR fluid containing nanorod-shaped magnetite as magnetic filler, the possibility of appearance of nanoparticles agglomerates within the studied fluids will be object of further discussion.

Fig. 10 shows a direct comparison of the yield-stress, the consistency parameter and the pseudo-plasticity index (obtained from Herschel-Bulkley fluid model fitting) behavior according to the morphology of the magnetite filling nanoparticles. For this purpose and considering only the concentration of 5 %vol., the evolution of these parameters as a function of the applied magnetic field's strength is shown.

To sum up, the MR fluids fabricated with spherical and octahedral magnetite nanoparticles (both with similar size and saturation magnetization values) show a more pronounced magnetorheological effect than the other fluids. This is reflected in a considerable variation of the yield stress and consistency parameter, both changing from a minimum value in the absence of magnetic field to a maximum value under high enough applied magnetic field. The effect of the different concentrations, 5 %vol. and 10 %vol., is clearly seen in Table 2, where relative changes in the measured yield stress of a 2644.5 % (5 %vol.) and 4260.9 % (10 %vol.) have been determined for the spherical magnetite nanoparticles containing fluid, and 392.9 % (5 %vol.) and 795.2 % (10 %vol.) relative changes for the fluid containing octahedral shaped magnetite nanoparticles.

Again, the previously described behavior is roughly followed by the MR fluid fabricated with the NRd-shaped particles. However, the effect of the different concentrations is now different, with relative changes in the measured yield stress of a 361.8 % (5 %vol.) and 171.5 % (10 %vol.). Elongated magnetic particles as NRd-shaped ones will always tend to align with their long direction parallel to the applied external field since the effect of internal demagnetizing factors along that direction is extremely low [21] (for long cylinders, ≈ 0). Thus, the increase in concentration of NRd-shaped particles within the fluid gives rise to the appearance of permanently-formed columnar structures mainly formed by particles attached side-to-side by their longest dimension, that at the same time hidden the rheological response under applied magnetic field.

Finally, the MR fluid containing truncated octahedral magnetite nanoparticles shows a quite moderate change in the measured yield stress values (for zero and maximum applied magnetic field strengths) of only 95 % and 77.8 % for 5 %vol. and 10 %vol. concentrations, respectively. Even more, this relative change is lower for the fluid containing the 10 %vol. nanoparticles concentration. The formation of permanent octahedral nanoparticles agglomerates within the fluid based could be behind those previous observations, a situation that will be further unveiled.

3.2. Dimensionless analysis

MR fluids under applied magnetic field behave as strongly shear thinning materials with a viscosity that decreases with shear rate value. There are many examples of experimental viscosity data (see, for example [23–25]) measured at different shear rates and magnetic field intensities that typically collapse when plotted as a function of only the well-known Mason number. This experimental observation suggests that this number efficiently reflects the scaling or competition between both hydrodynamic and magnetostatic forces: while hydrodynamic forces tend to break the magnetic field-induced structures, the magnetic

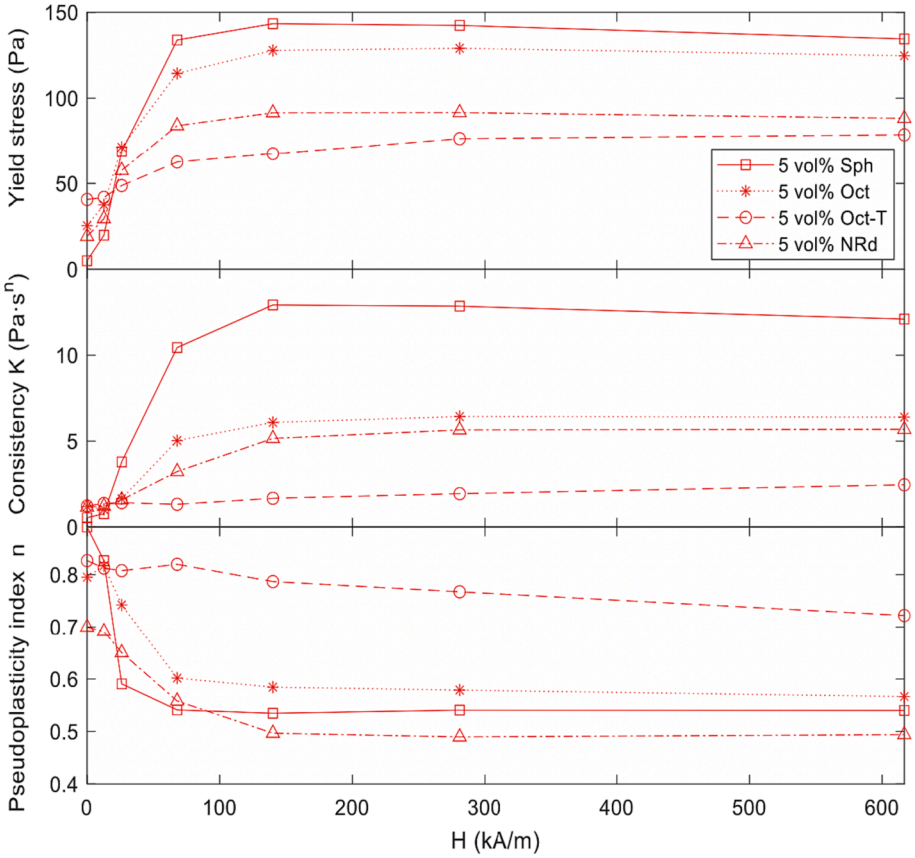

Fig. 10. Direct comparison of the obtained Herschel-Bulkley fitting parameters plotted against the the magnetic field strength only for the 5 %vol. particle concentration fabricated fluids and containing octahedral (Oct), truncated octahedral (Oct-T), rod-shaped (NRd) and spherical (Sph) magnetite nanoparticles. Measurements performed at room temperature.

dipolar interaction forces among particles try to keep them intact [26]. To deepen into the analysis of the behavior of the internal structures of our synthetized magnetic fluids in a comparative way, we performed a dimensionless analysis that will be discussed in this section. For this purpose, the dimensionless viscosity must be considered, which relates the apparent viscosity η_{app} for each point of the flow curve with the respective viscosity at the highest strain rate in the absence of magnetic field, η_∞:

$$Dimensionless\ viscosity = \frac{\eta_{app}}{\eta_\infty} \tag{2}$$

On the other hand, Zubarev *et al.* [26] definition of Mason number allows for an adequate representation of experimental results in the broad range of the magnetic fields:

$$Mn(M) = \frac{9}{2}\frac{\eta_c \dot{\gamma}\phi^2}{\mu_0 \mu_c \langle M\rangle^2} \tag{3}$$

where η_c and μ_c are the viscosity and permeability of the carrier liquid (also considering additives), ϕ is the volumetric concentration of the solid phase, and $\langle M\rangle$ is the suspension magnetization. Following this dimensionless analysis, it is possible to identify the two mechanisms of destruction of the internal structures: a) destruction by the bulk mechanism occurs when the hydrodynamic tension and the tension of magnetic forces exceed the compressive surface tension (the structures break into small parts leading to bulk movement); b) destruction by erosion (magnetic particles are worn from the surface of the structures due to hydrodynamic forces).

Fig. 11 shows the dimensionless diagrams of the four magnetic fluids formulated with 5 % volume concentration. It is clear than in all cases the flux curves at different magnetic field intensities tend to collapse in a single line.

Table 3
Slope of the dimensionless viscosity plotted against the Mason number for the studied magnetic fluids with % 5 vol concentration.

Particles shape	Slope
Octahedral	−0.862
Truncated octahedral	−0.857
Rod-shaped	−0.877
Spherical	−0.849
Mean ± standard deviation	−0.8613 ± 0.0118

Table 3 summarizes the slopes obtained by a single linear fit of all dimensionless points, for each fluid with 5 %vol. concentration of nanoparticles. All these fluids tested present a very similar slope ranging from −0.849 to −0.877, with mean value of −0.86 ± 0.01.

As observed by Zubarev *et al.* [26], the bulk destruction mechanism presents a power-law $\propto Mn^{-2/3}$ (slope: −0.666) behaviour and the erosive destruction scenario provides another scaling for the field-specific viscosity $\propto Mn^{-4/5}$ (slope: −0.8). According to the slope values obtained in this study, we have to consider that for our fluids, in all cases the dominant mechanism is destruction by erosion.

3.3. Observed reversibility

To end this exhaustive study, an analysis of the reversibility of the fluids was carried out. For this purpose, flow curves have been obtained in the absence of magnetic field after subjecting the sample to periods of different magnetic field strengths and a subsequent demagnetization cycle. As an example, Fig. 12 shows the results obtained for the fluid with spherical nanoparticles and a concentration of 10 %vol.

To facilitate the comparison among the different fluids, a parameter

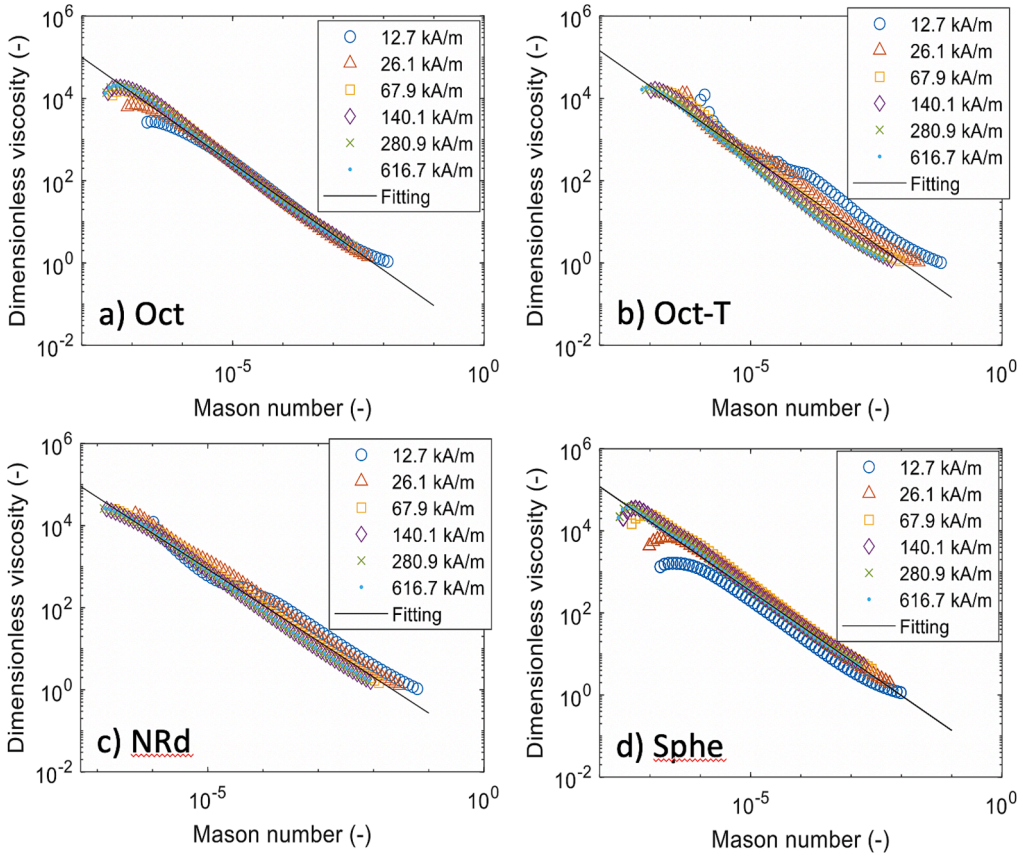

Fig. 11. Dimensionless viscosity plotted against the Mason number for magnetic fluids with 5 %vol. concentration; a) octahedral; b) truncated octahedral; c) rod-shaped; d) spherical. Measurements performed at room temperature.

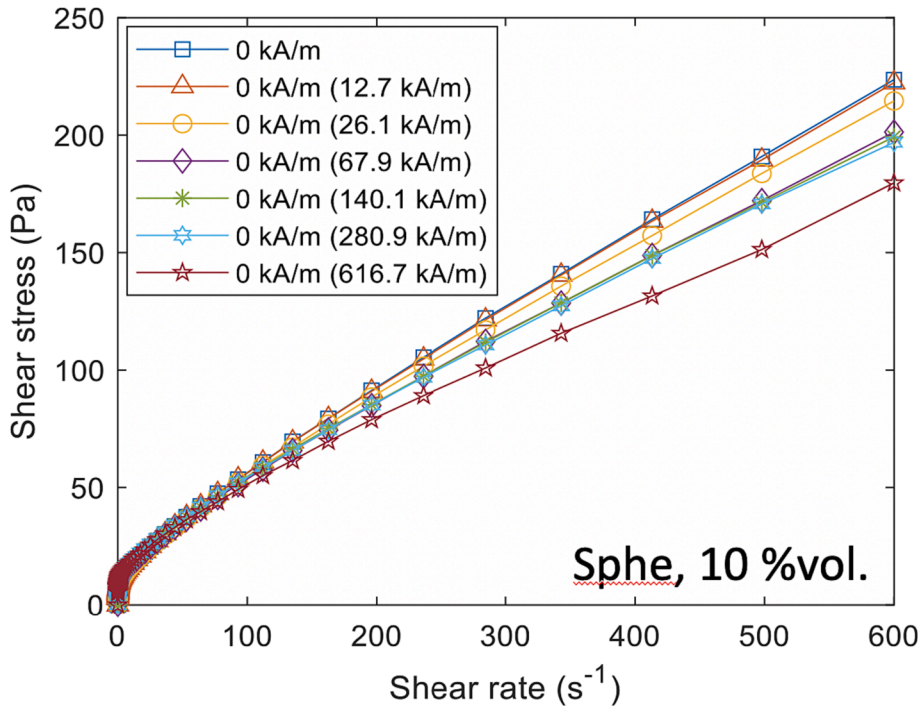

Fig. 12. Rheological curves of the magnetic fluid containing 10 % vol. spherical magnetite particle concentration after applying different magnetic field intensities and subsequent demagnetizing processes. Measurements performed at room temperature.

representing the reversibility capacity of the fluid can be defined by means of the following expression [27]:

$$Reversibility(\%) = (1 - \frac{\tau_{max} - \tau'_{max}}{\tau_{max}}) \times 100 = (\frac{\tau'_{max}}{\tau_{max}}) \times 100 \quad (4)$$

where τ_{max} is the shear stress at the maximum strain rate at 0 kA/m, and τ'_{max} is the shear stress at the maximum strain rate at 0 kA/m after being subjected to different intensities of the applied magnetic field and subsequent demagnetizing processes. Table 4 shows the values of τ_{max}, τ'_{max} and *Reversibility* (%) for each fluid and concentration.

A common trend for magnetic fluids based on octahedral, truncated octahedral and spherical magnetite nanoparticles is that the higher the magnetic field to which the fluid is subjected, the subsequent shear stress measured curve at 0 kA/m (after demagnetization) shows a downward trend ($\tau'_{max} < \tau_{max}$). As a representative case, in the observed reversibility curves of Fig. 12, after the application of the highest magnetic field (616.7 kA/m) there is a sudden reduction in the shear stress required to deform the MR fluid. Initially, spherical particles can align easily in the direction of the applied magnetic field (see Fig. 5). However, the clusters of particles that can also be present within the fluid do not achieve such good column structuring, causing the magnetic particles to be less strongly bounded and consequently, making easier to break these particles chains. This fact reflects in the shear stress required at 616.7 kA/m for the MR fluid to flow, that is lower than that needed at 241 kA/m as it was shown previously in Fig. 5.

More specifically, magnetic fluids based on octahedral and truncated octahedral nanoparticles exhibit the highest reversibility capacity (about a 92 %), with values that hardly vary with concentration. This high degree of reversibility is also favored by the low M_R/M_S ratio of 0.1 and 0 for the octahedral and truncated octahedral nanoparticles, respectively (see Table 1). On the other hand, the fluid based on spherical particles shows a lower reversibility capacity (70–80 %). Despite the previously good rheological behavior exhibited by the fluid containing this morphology of magnetite particles, they have the maximum measured magnetic saturation value (95 Am^2/kg) that leads to the highest magnetic dipolar interaction among nanoparticles that favors the appearance of nanoparticles agglomerates. However, the M_R/M_S ratio is now of 0.22 and this will hamper any reversible process within the corresponding fluid.

The measured reversibility curves for the fluid fabricated with NRd-like magnetite fillers shows un upward trend ($\tau'_{max} > \tau_{max}$), in opposite trend to the previously observed ones. This gives values of the reversibility above the 100 %, which can be explained as follows: the saturation magnetization of this type of nanoparticles is 40.7 Am^2/kg, the lowest one of the nanoparticles studied in this work. This makes the dipolar magnetic interaction among these magnetic rods to be the weakest one of all fabricated fluids. On the other hand and as previously reasoned, due to the low demagnetizing inner factor, these NRd shaped magnetite nanoparticles will easily align in the direction of any applied magnetic field. So, to apply a high intensity magnetic field (H_0) and subject the fluid to demagnetization has the effect of not completely destroying (remember the measured yield stress values for zero applied magnetic field) the induced columnar structure and they subsequently form a more stable one with the following applied magnetic field intensity ($H_1 > H_0$). This process can continuously improve the field-induced inner columnar structures and as a consequence enhance the reversible behavior of the fluid.

As previously demonstrated by the authors, the presence of aggregates of magnetic fillers within a MR fluid plays its role in the observed magnetorheological behavior [27]. To unveil the formation of

Table 4
Reversibility values for different magnetic fluids and concentrations.

Particles shape	% vol.	τ_{max} (Pa)	τ'_{max} (Pa)	$(\tau_{max} - \tau'_{max})$ (Pa)	Reversibility (%)
Octahedral	5	219.3	203.2	16.1	92.6
	10	311.9	288.5	23.4	92.5
Truncated octahedral	5	282.4	261.7	20.7	92.6
	10	488.1	444.2	43.9	91
Rod-shaped	5	121.5	128.6	− 7.1	105.8
	10	407.1	464.4	− 57.3	114.1
Spherical	5	167.1	119.7	47.4	71.6
	10	223.6	179.7	43.9	80.4

permanent nanoparticles agglomerates within our studied MR fluids, Small Angle X-rays (SAXS) measurements in all the MRF fluids fabricated with a 5 %vol. concentration of magnetic filler particle were performed. Obtained raw data were corrected firstly by making the background data subtraction and slit correction. Further, these processed data were evaluated by using Smart-Lab Studio II with MRSAXS plugin from Rigaku Corporation. Sphere or cylinder model for particles in oil matrix were used. Simulations were performed from 0.1 to 2°, with constant background and optimizing average diameter, size distribution, scale factor and packing fraction.

Fig. 13 shows the obtained filler particle size distribution for each of the fluids, while Table 5 summarizes the most relevant parameters obtained from these fits.

From these parameters we can conclude the following: the particle size distribution tells us that between D_{10} and D_{90} size values we will find enclosed the particles sizes of each magnetic filler. These values obtained from the fits agree with sizes obtained from TEM observations, and it is worthy to note that in the case of the spherical magnetite nanoparticles, most of them lie in the range of 33 ± 20 nm, and not in the 90 ± 10 nm one. But what is still more interesting is the value obtained for the packing fraction of the magnetic fillers within each fluid: in the case of octahedral and truncated octahedral filler nanoparticles, this is as low as less than 1 %. However, for nanorod and spherical magnetic fillers, this packing fraction value goes over a 40 %.

Clearly, SAXS technique results indicate that, at the low 5 %vol. concentration, octahedral and truncated octahedral filler nanoparticles do not aggregate within each correspondent fluid, while on the contrary nanorod and spherical magnetic fillers aggregate. This fact fully agrees with our previous observations: octahedral and truncated octahedral filler nanoparticles have a single domain structure with almost superparamagnetic behavior, the obtained packing fraction when playing within a MR fluid is extremely low (below 1 %) and as a consequence the observed reversibility is high (over a 90 %). On the contrary, the spherical magnetite nanoparticles are multidomain nanoparticles, the obtained packing fraction within a MR fluid is high (over 40 %) and so the measured reversibility lower (over a 70–80 %) than the previous ones. Finally, the nanorod shaped magnetite nanoparticles have also a single domain structure but the lowest saturation magnetization (lowest magnetic dipolar interaction between particles) of all the magnetic fillers studied. Nevertheless, the obtained packing fraction is high (over 40 %) and the reversibility observations indicate an inner process in the fluid that upon application of magnetic field causes a continuous

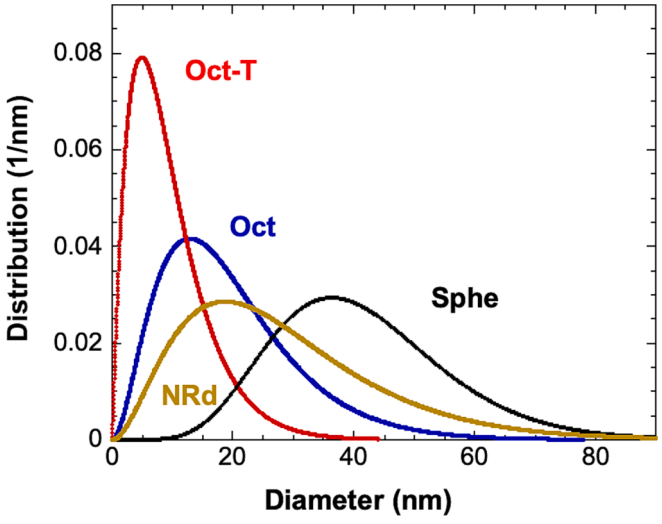

Fig. 13. Obtained filler particle size distribution from SAXS measurements, for each of the fluids with 5 %vol. nanoparticle content. Measurements performed at room temperature.

Table 5
Main parameters obtained from SAXS measurements fit.

	Oct Octahedral	**Oct-T** Truncated octahedral	**NRd** Rod-shaped (aspect ratio: L/D = 10)	**Sphe** Spherical
Average diameter (nm)	19	9	28	41
D_{10} (nm)	7	3	10	24
D_{50} (nm)	17	8	25	40
D_{90} (nm)	35	18	50	60
Mode diameter (nm)	13	5	19	36
Size distribution RSD (%)	58	69	58	35
Packing Fraction (%)	< 1	< 1	43	44

improvement of the field-induced inner columnar structures. In this case most probably the high packing fraction observed arises from the easy alignment of the magnetite rods along the direction of the applied magnetic field combined with the weak magnetic dipolar interaction among different magnetite nanorods.

4. Conclusions

In this work magnetic fluids of two different volume concentrations (5 % and 10 %) of magnetite nanoparticles with different morphologies (octahedral, truncated octahedral, rod-like and spherical) were formulated and fabricated to evaluate the influence of their diverse morphology on the magnetorheological behavior of the fabricated fluids. The results obtained allowed us to conclude that morphology, magnetic properties and concentration of magnetic fillers within a MRF play their role:

- The fluid with spherical nanoparticles presents the highest measured magnetorheological response, for both the concentrations studied. This arises on the one hand from their highest magnetic saturation, and on the other hand, due to an effective aggregation into nanoparticle clusters (44 % from SAXS measurements). The yield stress threshold is also the lowest measured one. However, this fluid presents low reversibility, most probably arising from the multidomain magnetic character combined with the easy aggregation of these nanoparticles morphology that gives rise to the observed large packing fraction within the fluid.
- The fluid based on octahedral particles (close in size and similar in saturation magnetization value to the spherical ones) exhibits a good balance between magnetorheological response and reversibility, which hints for the competitiveness of these particles for the formulation of magnetic fluids. However, this MRF higher yield stress threshold that the MRF fabricated with spherical nanoparticles of magnetite.
- On the contrary, truncated octahedral nanoparticles, although maintaining the good reversibility capability, present the poorest MR response among the four different nanoparticles morphologies studied. Besides, to increase the concentration of the magnetic filler worsen the measured MR response, despite aggregation has been estimated lower than 1 % in SAXS experiments.
- Nanorod-like magnetite particles containing MR fluid exhibit a good MR response that worsens when increasing the magnetite NRd concentration. The reversibility values obtained for rod-like particles together with the observed packing fraction (43 %) within the fluid indicate that a further deepening into the understanding of their dispersion and internal structuring is needed.
- All the fluids analyzed, regardless of the morphology of the nanoparticles, showed a preference for the erosion destruction mechanism.

CRediT authorship contribution statement

A. Gómez: Conceptualization, Supervision, Methodology, Validation, Writing – original draft and Review. **A. Barón:** Supervision, Methodology, Validation. **J. Berasategi:** Conceptualization, Supervision, Methodology, Validation, Data curation, Writing. **M. Blanco:** Supervision, Methodology, Validation. **A. García:** Supervision, Methodology, Validation. **J. Gutiérrez:** Validation, Data curation, Writing – original draft and Review. **D. Iglesias-Rojas:** Supervision, Methodology, Validation. **M. Insausti:** Supervision, Methodology, Validation, Writing. **S. Lanceros-Mendez:** Validation, Data curation, Writing. **C.R. Tubio:** Supervision, Methodology, Validation. **M.M. Bou-Ali:** Conceptualization, Supervision, Methodology, Data curation, Validation.

Declaration of competing interest

The authors declare that they have no known competing financial interests or personal relationships that could have appeared to influence the work reported in this paper.

Data availability

Data will be made available on request.

Acknowledgements

A. Gómez and A. García want to thank the Basque Government for funding under an FPI grant (PRE_2022_2_0277 and PRE_2022_2_0046, respectively). A. Gómez, J. Berasategi and M. Bou-Ali gratefully acknowledge the financial support of the Basque Government under Research Groups Programme (IT1505-22) and the Gipuzkoa Provincial Council under the Hoztikor (2022-CIEN-000052-01) projects. J. Gutiérrez and M. Insausti gratefully acknowledge the financial support of the Basque Government under Research Groups Programme (IT1479-22 and IT1546-22, respectively) projects. A. Baron, M. Insausti and D. Iglesias-Rojas also want to acknowledge the Spanish Ministry of Science and Innovation for financial support under grant No. PID2022-136993OB-I00 (AEI/FEDER, UE), funded by MCIN/AEI/ 10.13039/501100011033 and, as appropriate, by "ERDF A way of making Europe", by the "European Union". All the authors would like to thank the financial support provided by the Basque Government under research project MMASINT (KK-2023/00041, Elkartek Program). Technical and human support provided by the General Research Services of the UPV/EHU (SGIker) is gratefully acknowledged. In particular, fruitful discussions with A. Larrañaga are truly appreciated.

References

[1] J.D. Carlson, M.R. Jolly, MR fluid, foam and elastomer devices, Mechatronics 10 (2000) 555–569, https://doi.org/10.1016/S0957-4158(99)00064-1.
[2] F. Goncalves, A Review of the State of the Art in Magnetorheological Fluid Technologies - Part I: MR fluid and MR fluid models, Shock Vib. Dig. 38 (2006) 203–219.
[3] J. De Vicente, D.J. Klingenberg, R. Hidalgo-Alvarez, Magnetorheological fluids: a review, Soft Matter 7 (2011) 3701–3710, https://doi.org/10.1039/c0sm01221a.
[4] P.P. Phulé, J.M. Ginder, The materials science of field-responsive fluids, MRS Bull. 23 (1998) 19–21.
[5] S.W. Charles, "The preparation of magnetic fluids in Ferrofluids", Stefan Odenbach (Ed.): LNP, vol. 594, 3–18, 2002.
[6] G.M. Kamath, N.M. Wereley, M.R. Jolly, Characterization of magnetorheological helicopter lag dampers, J. Am. Helicopter Soc. 44 (1999) 234–248, https://doi.org/10.4050/JAHS.44.234.
[7] J. Berasategi, A. Gomez, M.M. Bou-Ali, J. Gutiérrez, J.M. Barandiarán IV, AP. S. Beketov, G.V. Kurlyandskaya, Fe nanoparticles produced by electric explosion of wire for new generation of magneto-rheological fluids, 8 pp, Smart Mater. Struct. 27 (2018) 045011, https://doi.org/10.1088/1361-665X/aaaded.
[8] V. Vadillo, A. Gómez, J. Berasategi, J. Gutiérrez, M. Insausti, I. Gil de Muro, J. S. Garitaonandia, A. Arbe, A. Iturrospe, M.M. Bou-Ali, J.M. Barandiarán, High magnetization FeCo nanoparticles for magnetorheological fluids with enhanced response, Soft Matter 17 (2021) 840–852, https://doi.org/10.1039/d0sm01702g.
[9] B.D. Chin, J.H. Park, M.H. Kown, O.O. Park, Rheological properties and dispersion stability of magnetorheological (MR) suspensions, Rheologica Acta 40 (2001) 211–219, https://doi.org/10.1007/s003970000150.
[10] H. Nishiyama, K. Katagiri, K. Hamada, K. Kikuchi, K. Hata, P. Sang-Kyu, M. Nakano, Evaluation of cluster structure and magneto-rheology of MR suspensions, Int. J. Mod. Phys. B 19 (2005) 1437–1442, https://doi.org/10.1142/S0217979205030414.
[11] R.C. Bell, J.O. Karli, A.N. Vavreck, D.T. Zimmerman, G.T. Ngatu, N.M. Wereley, "Magnetorheology of submicron diameter iron microwires dispersed in silicone oil", Smart Mater. Struct., vol. 17, 015028 (6 pp), 2008; doi: 10.1088/0964-1726/17/01/015028.
[12] J. De Vicente, J.P. Segovia-Gutiérrez, E. Andablo-Reyes, F. Vereda, R. Hidalgo-Alvarez, "Dynamic rheology of sphere- and rod-based magnetorheological fluids", J. Chem. Phys., vol. 131, 194902 (10 pp), 2009; doi: 10.1063/1.3259358.
[13] J. De Vicente, F. Vereda, J.P. Segovia-Gutiérrez, M. Puerto Morales, R. Hidalgo-Alvarez, Effect of particle shape in magnetorheology, J. Rheol. 54 (2010) 1337–1362, https://doi.org/10.1122/1.3479045.
[14] K. Nader, I. Castellanos-Rubio, I. Orue, D. Iglesias-Rojas, A. Barón, I. Gil de Muro, L. Lezama, M. Insausti, "Getting insight into how iron(III) oleate precursors affect the features of magnetite nanoparticles", J. Solid. State Chem., vol. 316, 123619 (8 pp), 2022; doi: 10.1016/j.jssc.2022.123619.
[15] I. Castellanos-Rubio, O. Arriortua, D. Iglesias-Rojas, A. Barón, I. Rodrigo, L. Marcano, J.S. Garitaonandia, I. Orue, M.L. Fdez-Gubieda, M. Insausti, A Milestone in the Chemical Synthesis of Fe3O4 Nanoparticles: Unreported Bulk-like Properties lead toa Remarkable Magnetic Hyperthermia, Chem. Mater. 33 (2021) 8693–8704, https://doi.org/10.1021/acs.chemmater.1c02654.
[16] N. Miguel-Sancho, O. Bomatí-Miguel, G. Colom, J. Pablo Salvador, M. Pilar Marco, J. Santamaría, Development of Stable, Water-Dispersible, and Biofunctionalizable Superparamagnetic Iron Oxide Nanoparticles, Chem. Mater. 23 (2011) 2795–2802, https://doi.org/10.1021/acs.chemmater.cm1036452.
[17] J.-C. Si, Y. Xing, M.-L. Peng, C. Zhang, N. Buske, C. Chen, Y.-L. Cui, Solvothermal synthesis of tunable iron oxide nanorods and their transfer from organic phase to water phase, Crys. Eng. Comm. 16 (2014) 512–516, https://doi.org/10.1039/C3CE41544A.
[18] Q. Li, C.W. Kartikowati, S. Horie, T. Ogi, T. Iwaki, K. Okuyama, Correlation between particle size/domain structure and magnetic properties of highly crystalline Fe3O4 nanoparticles, Scientific Reports 7 (2017) 9894, https://doi.org/10.1038/s41598-017-09897-5.
[19] T.G. Mezger, The rheology handbook, Vincentz Network, Germany, 2002.
[20] G. Bossis, P. Kuzhir, S. Lacis, O. Volkova, Yield stress in magnetorheological suspensions, J. Magn. Magn. Mater. 258–259 (2003) 456–458.
[21] S. Chikazumi, Physics of Ferromagnetism, 2nd Edition, Oxford University Press, USA, 1997.
[22] A. Saasen, J.D. Ytrehus, Viscosity models for drilling fluids - Herschel-Bulkley parameters and their use, 16 pp, Energies 13 (2020) 5271, https://doi.org/10.3390/en13205271.
[23] O. Volkova, G. Bossis, M. Guyot, V. Bashtovoi, A. Reks, Magnetorheology of magnetic holes compared to magnetic particles, J. Rheol. 44 (2000) 91–104.
[24] J. Ramos, D.J. Klingenberg, R. Hidalgo-Alvarez, J.deVicente, "Steady shear magnetorheology of inverse ferrofluids", J. Rheol. 55 (2011) 127–152, https://doi.org/10.1122/1.3523481.
[25] D.W. Felt, M. Hagenbuchle, J. Liu, J. Richard, J. Intell. Mater. Syst. Struct. 7 (1996) 589–593.
[26] A. Zubarev, L. Iskakova, P. Kuzhir, G Bossis On the theory of magnetoviscous effect in magnetorheological suspensions, J. Rheol. 58 (2014) 1673–1692, https://doi.org/10.1122/1.4886175.
[27] J. Gutiérrez, V. Vadillo, A. Gómez, J. Berasategi, M. Insausti, I. Gil de Muro, M. Bou-Ali, "Aspects concerning the fabrication of magnetorheological fluids containing high magnetization FeCo nanoparticles", Fluids vol. 6, 132 (11 pp), 2021; doi:10.3390/fluids6030132.